2.4 GHz circularly-polarized patch antenna for the AcubeSAT mission

AcubeSAT-COM-G-011

Electra Karakosta-Amarantidou
Afroditi Kita
Dimitris Stoupis

October 4, 2020
Version: 2

Aristotle University of Thessaloniki

Aristotle Space and Aeronautics Team
CubeSat Project

2020

Contents

Appendices

Changelog

Date	Version	Document Status	Comments
4/10/2020	2	PUBLISHED	Extracted new diagrams for the Simulations section. Added S11 measurements in Anechoic chamber testing. Added reference coordinate system
30/9/2020	1.4	DRAFT	Added the graphs for the phase and gain measurements. Also added content in the phase and gain results.
20/9/2020	1.3	DRAFT	Merged AcubeSAT-COM-EC-012. Reorganized some sections. Added text in the Construction section
05/05/2020	1.2	DRAFT	Added the structure of the document for the anechoic chamber tests. Also all the graphs for the antenna pattern and antenna gain were added.
18/04/2020	1.1	DRAFT	Antenna pattern measurement in anechoic chamber
17/11/2019	1.0	INTERNALLY RELEASED	First Release, including only the preliminary testing
15/11/2019	0.4	DRAFT	Added the final graphs, changing some of the names
15/06/2019	0.3	DRAFT	Included the experimental and theoretical graphs
30/05/2019	0.2	DRAFT	Added setup images and details about the equipment
25/05/2019	0.1	DRAFT	Initial revision

This is the latest version of this document (2) as of October 4, 2020. Newer versions might be available at `https://helit.org/mm/docList/public/AcubeSAT-COM-G-011`.

Reviewed and approved for public release by the Systems Engineering Team.

Acronyms

2D Two Dimensional

3D Three Dimensional

AUT Antenna Under Test

CAD Computer Aided Design

CP Circular Polarization

FR-4 Flame Retardant 4

HPBW Half Power Beam Width

ISM Industrial Scientific and Medical

LHCP Left Hand Circular Polarization

PCB Printed Circuit Board

RF Radio Frequency

UHF Ultra High Frequency

UV Ultra Violet

VHF Very High Frequency

VNA Vector Network Analyzer

References

[1] Amritesh and M. Singh. "Design of Square Patch Microstrip Antenna for Circular Polarization Using IE3D Software". In: 2009.

[2] Guesmi Chaouki et al. "An Electrical Model to U-Slot Patch Antenna with Circular Polarization". In: *International Journal of Advanced Computer Science and Applications* 8 (Mar. 2017). DOI: 10.14569/IJACSA.2017.080310.

[3] Edward Collett. *Field guide to polarization*. Bellingham, Wash: SPIE, 2005. ISBN: 9780819458681.

[4] Ramesh Garg. *Microstrip antenna design handbook*. Boston, MA: Artech House, 2001. ISBN: 0-89006-513-6.

[5] Mohd Jamlos et al. "2.3 GHz –2.45 GHz Circular Polarization U-Slot Patch Antenna". In: Sept. 2012. DOI: 10.1109/ISWTA.2012.6373824.

[6] John Kraus. *Antennas for all applications*. New York: McGraw-Hill, 2002. ISBN: 0072321032.

[7] Abdul Halim Lokman et al. "A Review of Antennas for Picosatellite Applications". In: *International Journal of Antennas and Propagation* 2017 (2017), pp. 1–17. DOI: 10.1155/2017/4940656. URL: http://dx.doi.org/10.1155/2017/4940656.

1 Introduction

This document details the design, construction and testing of a **2.4 GHZ, U-slot, circularly polarized microstrip antenna** that was based on the works [5] and [2].

This document is structured as follows. In section 2, the requirements imposed by the mission and the concluding requirements of the antenna are presented. Then, in section 3, a brief rationale about the choice of the specific antenna type is given. Moving on, the design process, containing the theoretical analysis for each element of the antenna, and the parameters that were used for modeling the antenna CAD in CST are included in section 4. In section 6, the steps that were followed for the construction of the first prototype of the antenna are listed. A first, preliminary testing of the prototype is described in section 7. Finally, the procedures, results and conclusions of the prototype testing in the anechoic chamber are presented in section 8.

From the moment we decided to use an in-house antenna for AcubeSAT until we conducted the last tests in an anechoic chamber around February 2020, almost 1.5 year has passed. Through this endeavor, the members of the Communications subsystem that were involved in the different phases of the development learned a great deal about the theory behind circular polarization, microstrip antennas, the difficulties of simulating, constructing and testing a model, as well as the differences between designing and actually making an antenna to be used in a real mission. After multiple design iterations, materials used and methods applied, we are presenting you the final design, hoping that this document can be enlighting for anyone willing to try something similar.

Note that the document is a constant work in progress. Whenever something new happens regarding the development of the antenna (e.g. construction of a new model, new testing iterations), it will be added here. Make sure that you are viewing the most updated version. You can also keep track of the changes in the Changelog above.

2 Requirements

2.1 Mission requirements

The main factors we took into consideration while selecting our payload's antenna were:

- **Size**: A small, compact antenna is needed in the case of a small spacecraft as AcubeSAT.
- **Available Power**: Regarding the power constrains, a higher gain might be essential.
- **Volume of the Payload data**: In case the communications window is limited, a higher rate is required; thus, a more directive antenna seems to be a preferential choice (taking into consideration the power constrains).
- **Downlink Frequency - Path Loss**: The higher the downlink frequency, the weaker the received signal becomes. According to the Friis Law, the path losses are increasing, therefore a higher antenna gain might be useful. From another point of view, as long as we use antennas acting as resonators[1], what mainly determines the size of the antenna is the resonant frequency. Last but not least, the available bandwidth and consequently the data rate are determined from the chosen band.
- **Nadir pointing deviation - Pointing Losses**: A directive antenna is more vulnerable to pointing losses. It depends on the accuracy of nadir pointing as well as on the beamwidth of the antenna.
- **Faraday's Rotation**: Circular polarization is required to avoid the aforementioned phenomenon in which the vector of the electric field is rotated in a random way while the wave travels through the atmosphere.

2.2 Antenna requirements

The above factors are partially dependent on each other, which becomes clear through the link budget calculation. To elaborate, Comms members made the following thoughts: AcubeSAT's payload data consists of images. This accidentally means that we need a high data rate and a higher bandwidth than VHF and UHF bands can provide. For the above reasons, we selected **S band (2.4-2.45 GHz)**. As a result, our spacecraft's antenna can be of a smaller size. The higher path losses and the limited power result to the need of a more directive antenna which is constrained by the pointing losses and the degree of deviation from nadir pointing. In order to create a **reliable downlink path** we end up with the following **requirements** which should be satisfied in the whole band of 2.4-2.45 GHz:

- **Resonant frequency between 2.4- 2.45 GHz**, wavelength: 12.5-12 cm. Reflection coefficient must be lower than -10db in the whole band.
- **Antenna Gain** of at least **5 dB**.
- **Circular Polarization**. Axial Ratio -3dB.
- **Half Power Beamwidth** of at least 80 degrees[2].

[1] Dipoles, microstrip patch
[2] The half power beamwidth of circular polarization should also satisfy the requirement

- **Small size**
- **Simple feeding circuit Low cost**

Our main challenge was achieving both **high gain** and **wide beamwidth**. Another was implementing **circular polarization** with a non-complex feeding circuit. To combat said issue, we resorted to achieving two orthogonal field components radiated with equal amplitude but in phase quadrature by different means, touched upon later on. Lastly, **lack of knowledge** regarding the procedure of designing a microstrip antenna further hindered, albeit not ceased, our efforts.

3 Rationale

The most common antennas used in CubeSat missions are the dipoles (especially in the UHF and VHF bands). **Dipoles** are omnidirectional antennas[3], with a gain of 2.17 dBi and a beamwidth of 75 degrees. Although simple and cheap, they require a deployment system.

Figure 1: *CubeSat in orbit with dipole antenna*

Some **parabolic dishes** have been also used and more information about that can be found in [7].

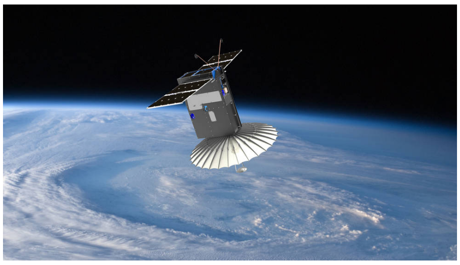

Figure 2: *CubeSat in orbit with a parabolic dish antenna*

Microstrip patch antennas predominantly appear on CubeSat missions utilizing S and X band when high data rate is required. They are **low-profile** antennas, consisting of a flat rectangular sheet or **"patch" of metal**, mounted over a larger sheet of metal called a **ground plane**. The patch and the ground are separated by a **dielectric substrate**. The value of λ in those frequencies is less than 10 cm and, consequently, mounting the antenna on the spacecraft's surface is feasible.

Summarizing, a **microstrip patch antenna was selected** to be mounted on the side facing the Earth, main reasons being:

- Low profile, light weight, low volume
- Ease of installation, no deployment system is needed
- A higher gain than that of dipoles can be achieved

[3] The use of dipoles ensures reliability of the communication datalink without the need of nadir pointing

- Circular polarization can be created without using two elements, but smart techniques such as cutting the edges of a square patch
- Variety of designs, slots can be used to make antenna size smaller
- Easy to fabricate and test[4]

[4] This does not comprise a design-related reason but still is an advantage.

4 Design

4.1 A brief summary

When we design a radiating patch, we are free to form every possible shape and examine its behaviour. Although this may sound useful, to imagine the electric field and the current distribution beforehand seems quite challenging. Thus, at first, we thouroughly studied previous research focused on these antennas, the theoretical analysis and the results that arise. Additionally, we focused on microstrip antennas designed or manufactured to be used on CubeSat missions.

After having studied the main theoretical analysis, we concentrated on designs that have similar requirements with our own and proceeded to apply some of the mathematical formulas and techniques, using the CST Studio Suite environment; a prolonged process of trial and error[5]. Finally, we created an antenna similar to the one presented in [5] and [2], adapting its parameters[6] to satisfy our requirements.

4.2 Theoretical Analysis

In this section two theoretical models of a patch antenna are presented and techniques applied are briefly discussed. It is worth mentioning that changing a parameter's value can severly affect some of the antenna's properties unexpectedly. Considering that we can modify each one of the parameters in the above figure, we have 9 degrees of freedom[7]. While this might seem exciting to some, since it allows for creative approaches, it subsequently contributes to the overall complexity, because maintaining control and comprehending how each value influences the model becomes accumulatively difficult.

The most usual **models** for the analysis of a microstrip patch antenna are the **transmission line**, the **cavity** and the **full wave** models. The reader is encouraged to study more about these models in [1] (or any other book related to antenna theory) in case they find this field compelling.

4.2.1 Resonance frequency-Bandwidth

As stated above, resonance frequency depends mostly on the size of the conducting area of the patch. Given the values of the height and the dielectric properties of the substrate, we can calculate the values of L, W by the formulas arised from the aforementioned models. Techniques as slots are used to further reduce the size of the patch.

4.2.2 Circular polarization (CP)

There exist many studies on obtaining circular polarization waves. Patches of square, circular, pentagonal, equilateral, triangular, ring, and elliptical shapes are capable of

[5] The most challenging part was to control the Axial Ratio value.
[6] Through extensive parametric analysis.
[7] Including the height of the substrate and position of the feed.

circular polarization operation. Note that **square and circular patches** are widely utilized in practice.

A **single patch antenna** can be made to radiate circularly polarized waves, if two orthogonal patch modes are simultaneously excited with equal amplitude and out of phase, with sign determining the sense of rotation. There are two types of feeding: the dual-orthogonal feed (which employs an external power divider network) and the **single point feed with the truncated corners.**

Concluding our design, we opted for the square patch and the truncated corners approach mainly for its simplicity. Because a patch with single-point feed generally radiates linearly polarized waves, in order to radiate CP, it is necessary for two orthogonal patch modes with equal amplitude and in-phase quadrature to be induced. This can be accomplished by slightly **perturbing a patch at appropriate locations with respect to the feed**. Perturbation configurations for generating CP operate on the principle of **detuning degenerate modes of a symmetrical patch by perturbation segments** as shown in Figure 3. The fields of a singly fed patch can be resolved into two orthogonal degenerates modes 1 and 2. Proper perturbation segments will detune the frequency response of mode 2 such that, at the operating frequency f_o, the axial ratio rapidly degrades while the input match remains acceptable.

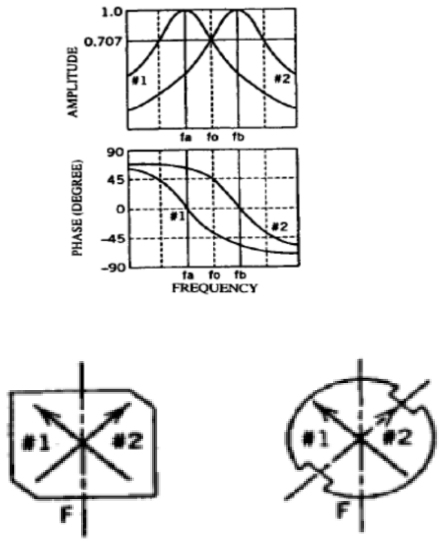

Figure 3: *Generating CP by detuning degenerate modes [4]*

When the upper left and the bottom right corner are truncated, the patch radiates **Left hand circular polarized waves**, **LHCP**. In our case the antenna radiates **Left Hand Circularly Polarized Waves**.

4.2.3 Dielectric Substrate

The substrate's **dielectric permittivity** usually takes values in the range $2.2 \leq \epsilon_r \leq 12$. A **low value** of ϵ_r results to:

- Enhanced efficiency
- Wider bandwidth
- Better radiation characteristics
- Larger height, length and width

In contrast, a **high value** of ϵ_r results to

- Smaller dimensions
- Less efficiency
- Narrow bandwidth

We decided to use **FR-4** because it is low-cost and widely produced. It is commonly used in PCBs as well as patch antennas. The electric permittivity for FR-4 can take values in the range of [4, 4.5]. We simulated our antenna using FR-4 with $\epsilon_r = 4.5$.

4.2.4 Multiple layers of substrate - Height of substrate

We applied the **multilayer substrate techinque** in order to achieve **larger bandwidth and higher gain**. However, in case the height is increased up to a certain point, the efficiency of the antenna and thus the gain deteriorate due to the spurious high order surface wave modes.

The custom FR-4 boards are usually produced with a height of 1.6mm or 3.2mm. In order to create a larger height, it is necessary to **stack different layers of FR-4** and that's what multilayering means.

4.2.5 U-slot

You may have noticed the **slot in the shape of the letter U** that makes our antenna happy. The designers in [5] describe: "The patch was loaded with a U-slot to **introduce a capacitance that can suppress the inductance due to the vertical feeding probe** so as to enhance the impedance and S_{11}". Additionally, the resonant frequency can be achieved with smaller dimensions.

4.3 Designing on CST environment

We used the **CST environment 2017** in order to design our antenna and examine its characteristics.

The dimensions of the CAD that was designed are summarized in Table I. For a better overview, the mechanical drawings of the final design can be found in Appendix A *(dimension annotation is also shown there)*.

***Table I**: Dimensions of the CST CAD model*

Parameter	Type	Value	Unit
h	Height of substrate	4.5	mm

e_r	Electric permittivity of the substrate	4.5	-
L	Length of radiating element	26.5	mm
W	Width of radiating element	26.5	mm
L_t	Length of truncated corners	5.6	mm
a	Distance of slot from lower edge of radiating element	6	mm
b	Length of slot	13	mm
y_{feed}	Vertical distance of feed from antenna center	7.66	mm
x_{feed}	Horizontal distance of feed from antenna center	0	mm
W_2	Width of slot	1.5	mm

The material assigned to the ground plane and radiating element was **Copper (pure)** and **FR-4** was assigned to the substrate. The characteristics of these materials can be found in tables II and III respectively.

Table II: *Characteristics of Copper (pure) used for simulations*

Copper (pure)	
Type	Lossy metal
Electric Conductivity	5.96×10^7 [S/m]
ρ	8930 [kg/m^3]
Thermal conductivity	401 [W/K/m]

Table III: *Characteristics of FR-4 used for simulations*

FR-4	
e_r	4.5
ρ	1850 [kg/m^3]
Thermal conductivity	0.3 [W/K/m]

5 Simulations

Using the model that was designed in CST, we performed simulations to determine the performance of the antenna with respect to the main characteristics of interest. The results are presented in the following paragraphs.

5.1 Frame of Reference

The first convention that we have to make is to define the frame of reference relative to the patch antenna, so that in all simulations and subsequent test results there is consistency as to what we denote as horizontal, vertical, left or right. Below in Figure 4, the 3D render with the defined axis can be found. The angles θ and ϕ are defined with respect with a random point P in 3D space. The origin lies in the ground plane (not depicted in Figure 4).

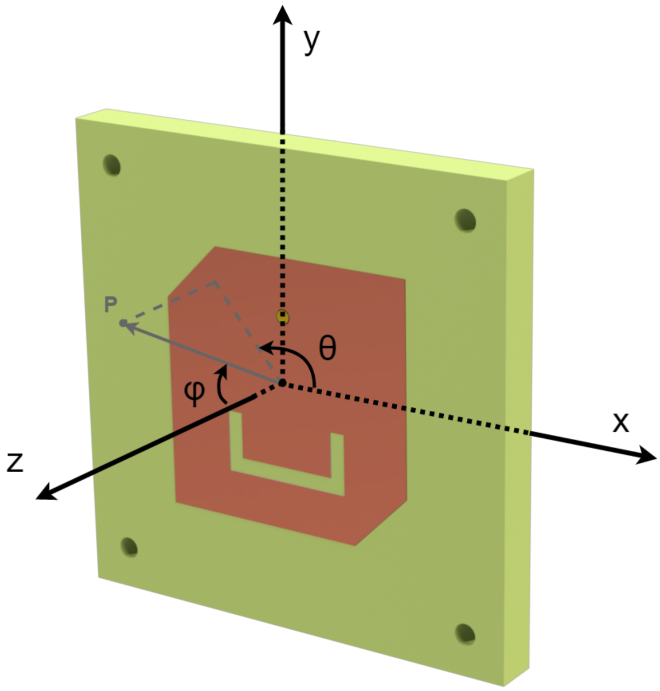

***Figure 4**: Frame of reference relative to the patch antenna*

5.2 Reflection Coefficient

As we can see in Figure 5, the reflection coefficient is less than -10dB in the whole range 2.28-2.6 GHz. Additionally, it is below -20 dB in the operational frequency range (2.4-2.45 GHz).

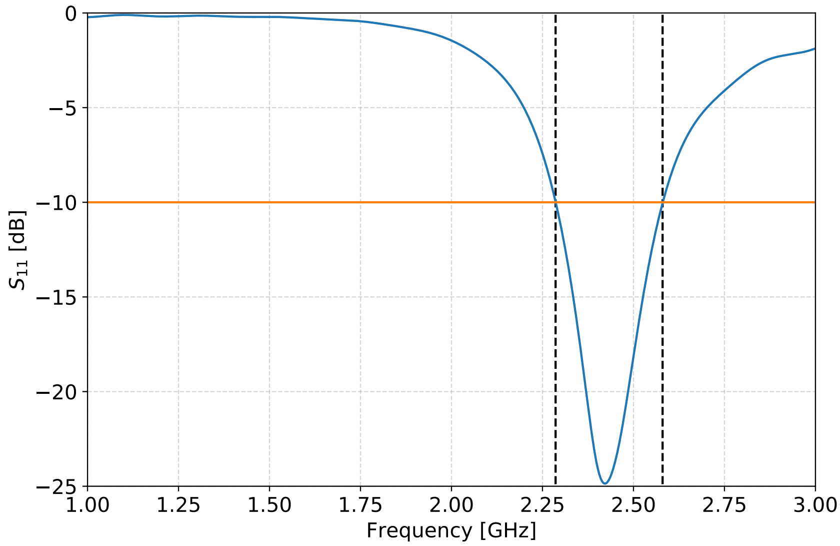

***Figure 5**: Reflection Coefficient*

5.3 Radiation Pattern - Gain - Efficiency - HBPW

The radiation pattern in the whole range of interest (2.4-2.45 GHz) has the typical shape of a "balloon".

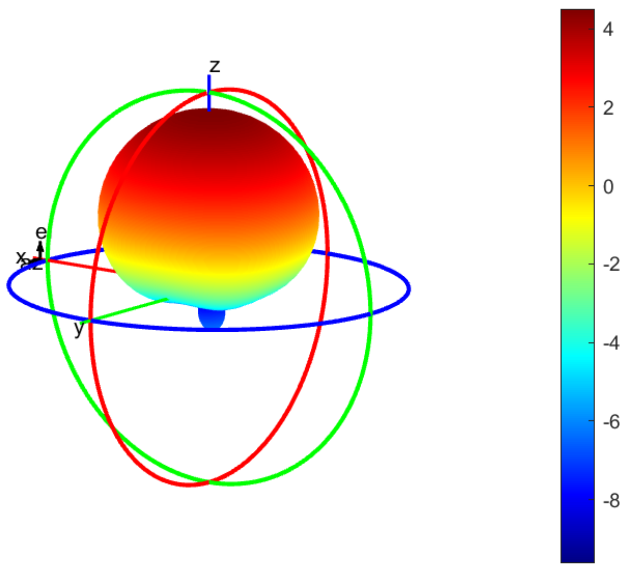

***Figure 6**: Far Field Radiation Pattern at 2.43 GHz*

What we can derive from Figure 6 are the shape of the main lobe and its direction at 2.43GHz. The **Gain has a value of 4.5 dB**. As we can see, the **total efficiency emerges to be 0.71**. The losses of the substrate due to its thickness and quality may have lead to this result.

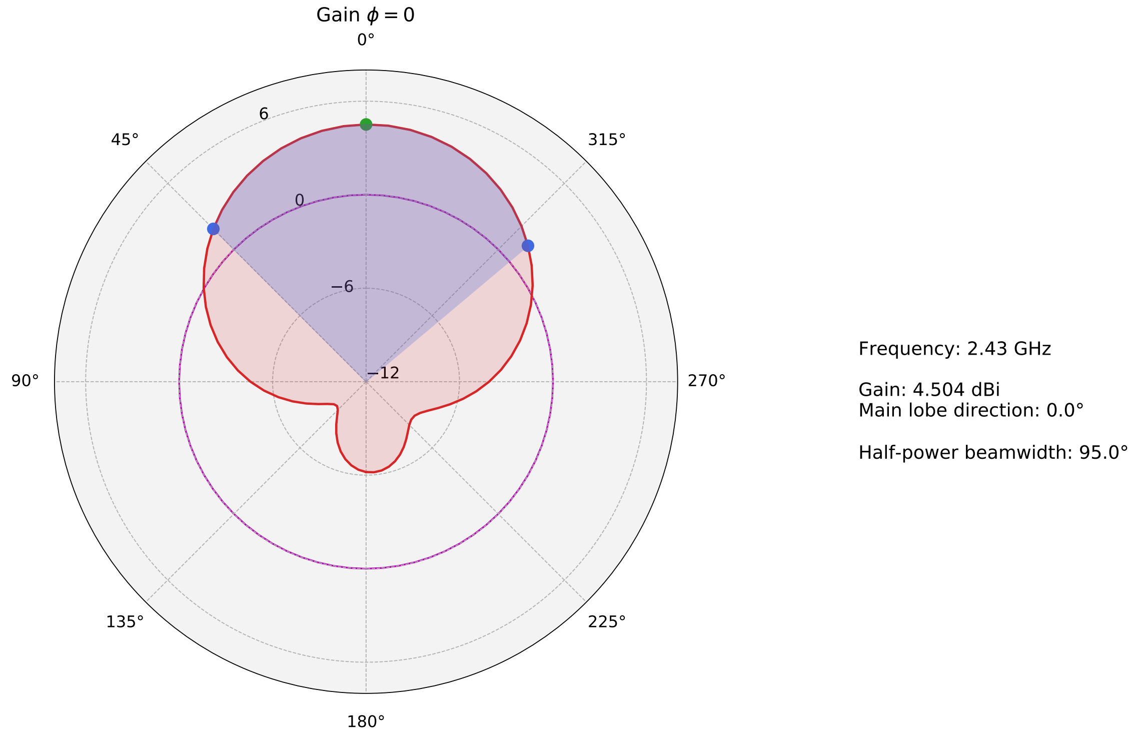

***Figure 7**: 2D polar pattern (gain) at $\phi = 0$*

From the polar diagram in Figure 7, it is clear that the **HPBW** is **95°** in 2.43GHz. Moreover, the **side lobe level is S_{LL}=-10.7 dB**. We need to keep in mind the antenna is mounted on the surface of the CubeSat. There are two important things to note. The aluminum surface may act as a reflector, suppress the side lobe and increase the total gain. Even if the gain will not be increased we need to examine the amount of the power inserted to the cubesat.

5.4 Gain - Beamwidth vs Frequency

The **Gain** arises to be **4.45-4.5** dB in the whole frequency range as we can see in Figure 8. We **did not satisfy** the requirement of a value higher than 5 dB. An idea that came up was to search and simulate materials that have less losses than FR-4. However, due to time constrains we decided to proceed and assemble this design.

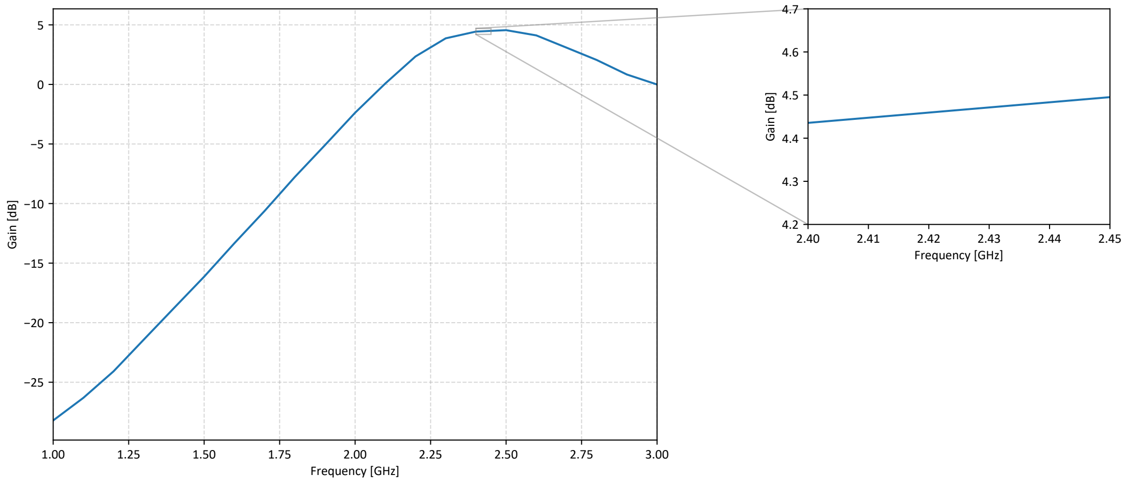

Figure 8: *Gain vs frequency*

5.5 Axial Ratio vs Frequency

It has already been mentioned that the value of Axial Ratio should be below 3 dB to obtain circular polarized waves. Note that the patch radiates **LHCP waves.**

In the whole range of **2.4-2.45 GHz the Axial Ratio is below 3dB**. The lower value appears at 2.43 GHz.

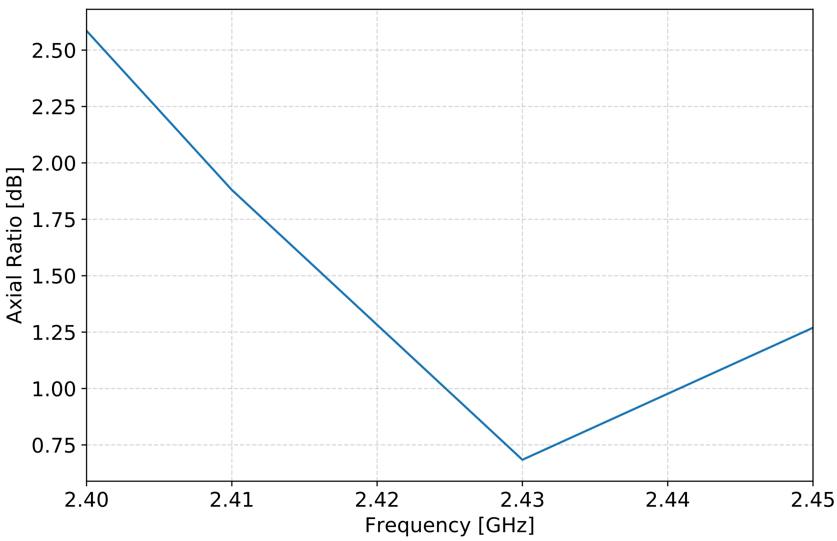

Figure 9: *Axial Ratio in the 2.4-2.45 GHz band*

5.6 Circular Polarization Beamwidth

We provide some more diagrams in 2.4GHZ and 2.45 GHz in order to examine the axial ratio as a function of the angle theta in the upper and lower frequency.

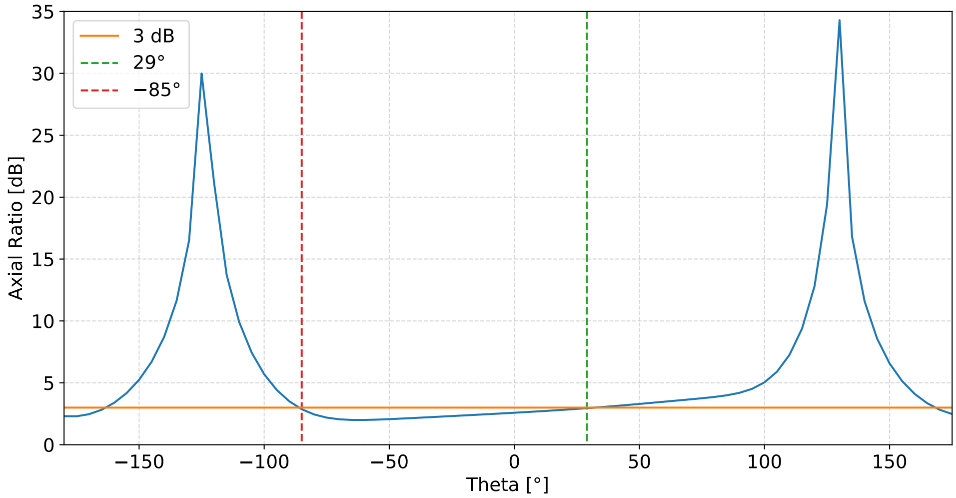

***Figure 10**: Axial Ratio vs angle theta at 2.4 GHz*

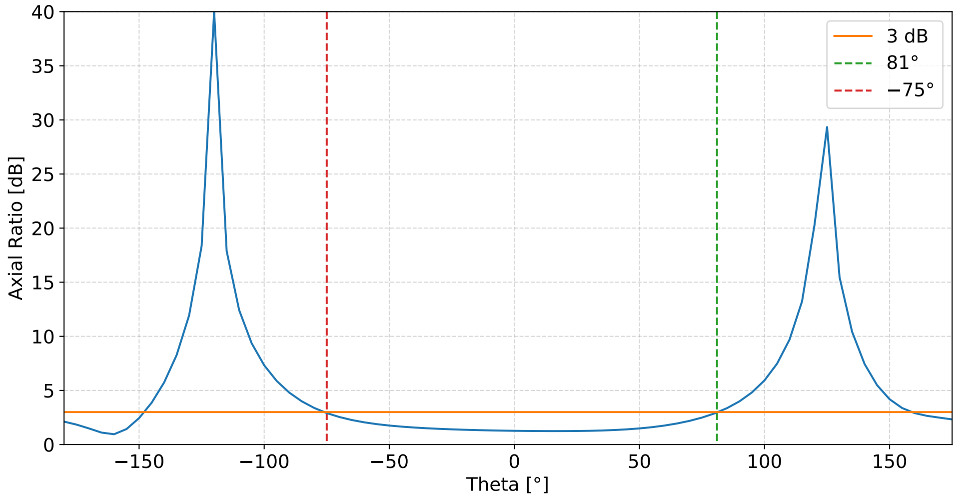

***Figure 11**: Axial Ratio vs angle theta at 2.45 Ghz*

As we can see in Figure 10, at 2.4 GHz the circular polarization beamwidth (the angle that axial ratio is below 3 dB) is **much more narrow** in comparison with 2.45 GHz (Figure 11).

6 Construction

After finalizing the dimensions of the model through the series of simulations described in the previous section, we proceeded on **constucting a first protoype** in ASAT's laboratory.

Due to the fact that the design of the antenna imposes a 4.5 mm thickness, the construction of the model in-house was not very trivial. Most of the FR-4 materials that are available on the market have a typical 1.5 mm thickness. Moreover, we needed one side of the substrate to have a photosensitive surface, in order to be able to create the design through UV light exposure. After an extensive research, we were not able to find an appropriate material readily available.

To overcome this issue, we used 3 layers of FR-4 instead:

- One layer with a photosensitive copper surface (top layer)
- One plain FR-4 layer (middle layer)
- One layer with a copper surface (bottom layer)

The procedure that we followed for the construction was:

1. At first, we cut the plain and ground layers to be closer to the wanted dimensions of the patch (Figure 12).

Figure 12: *Cutting the FR-4 boards*

2. Then, we used two part Epoxy resin to stick the two layers together and left them overnight to make sure that the adhesion would last. We applied pressure to remove any air bubbles that could potentially alter the antenna's characteristics. We also tried to use a solid Epoxy resin in order to form a layer, for uniformity purposes, but ended up using liquid Epoxy resin instead (Figure 13).

Figure 13: *Adhesion of the middle and bottom layer*

3. We extracted the Gerber file of the antenna and used it to print the design on the photosensitive FR-4 board, using our home-made UV box (Figure 14).

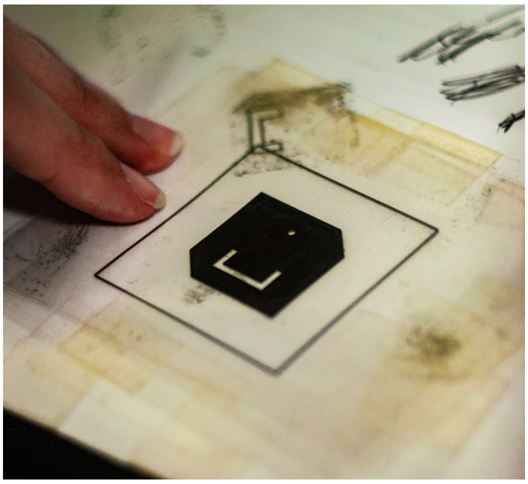

Figure 14: *The Gerber extraction for printing on the top layer*

4. We **etched** the board and then **developed** the design using the appropriate chemicals for each case (Figure 15).

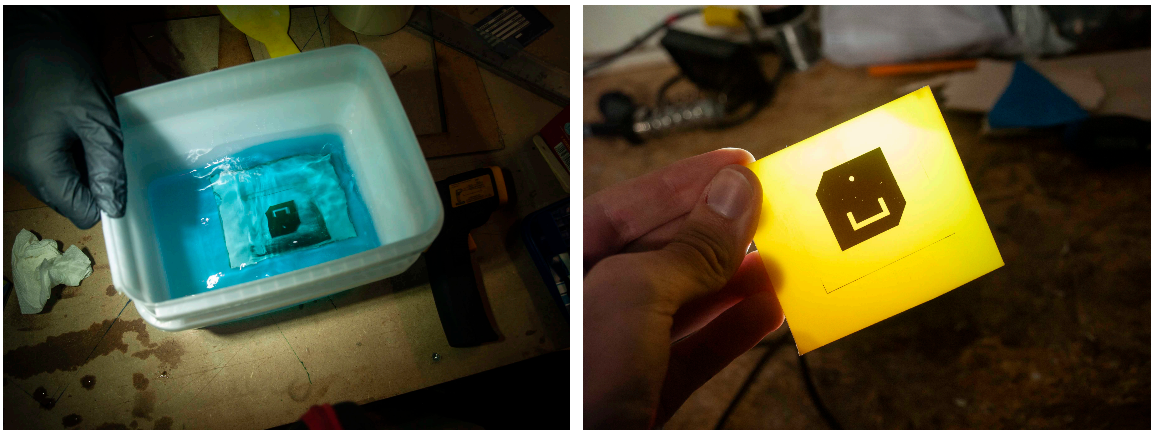

Figure 15: *Development process of the design on the photosensitive board and the result*

5. Afterwards, we proceeded on adhering the top layer, similarly to 2 (Figure 16).

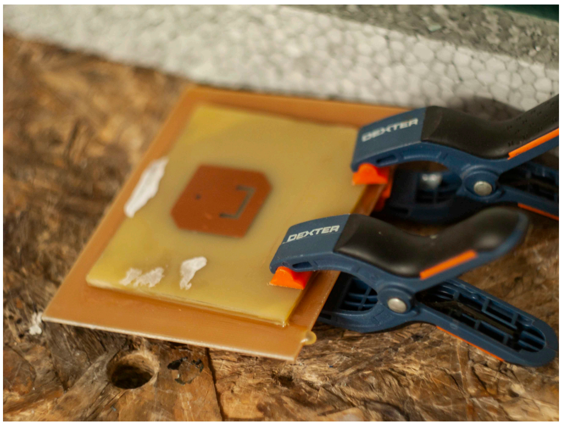

***Figure 16**: Adhesion of the top layer*

6. After the glue had completely dried, we measured the resulting thickness (Figure 17). There were some uneven points, but all in all the values were close to the desired 4.5 mm.

***Figure 17**: Measuring the thickness after adhesion of all layers*

7. We sanded the boards to the desired dimensions (Figure 18).

***Figure 18**: Sanding the adhered boards*

8. Lastly, we drilled a hole to connect a **chassis-mount SMA** connector to the antenna. Specifically, we soldered the inner conductor of the connector to the copper on the top layer and the metallic body of the connector to the bottom layer (ground plane).

The finished antenna can be seen in Figure 19.

Figure 19: *Front and back view of the completed antenna*

7 Preliminary testing

A first laboratory testing was conducted in order to evaluate the characteristics and theoretical performance of the 2.4 GHz, circular polarization patch antenna that the Communications subsystem has designed.

7.1 S Parameters

To measure the performance of an antenna we use the so-called **S Parameters**, with two numerical subscript indices, like S_{21}. The numerical indices indicate the transmission and reception direction, provided that we have two antennas. For example, the S parameter S_{21} indicates the power transferred from *antenna 1* to *antenna 2* in the setup, where the antenna numbering is set during the measurement. When the S parameter has the same index, like S_{11}, then the reflection coefficient or the tuning range of the corresponding antenna is measured, because we are measuring the portion of the power that is reflected back to the RF generator. Having the S parameters for an antenna under testing, we can determine its performance and draw useful conclusions.

7.2 Measurement conditions

The experimental setup was set inside an educational laboratory without any form of electromagnetic isolation or reflection absorption. Therefore the results of this test are deemed useful only as a preliminary approximation of the antenna's actual performance.

7.3 Measurement equipment

For the conclusion of the testings, Keysight Technology's *Agilent HP-8714ES* network analyzer was used. This network analyzer offers **1 Hz resolution**.

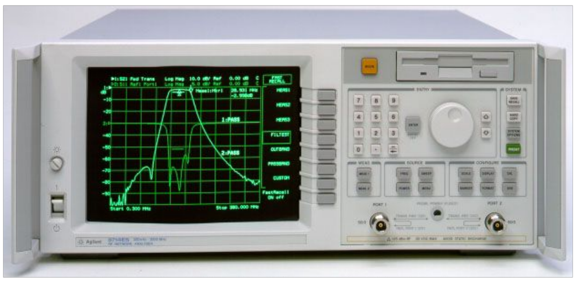

Figure 20: *Keysight Technology's network analyzer*

7.4 Transmission coefficient (S_{21}) measurement

7.4.1 Procedure

- Two horn antennas were connected facing each other.

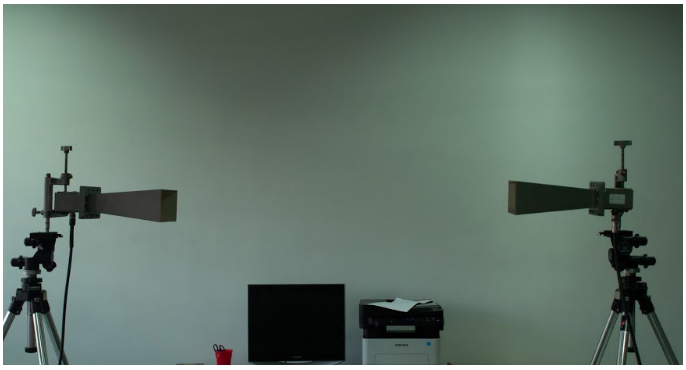

Figure 21: *Calibration with horns as a reference*

- Calibration was performed, not using the calibration kit, but assuming that a calibration signal between the two horn antennas corresponds to the 0 dB level.
- One of the horn antennas was disconnected and replaced by the patch antenna under test.

Figure 22: *Replacement of horn with the patch antenna*

- Measurements for different orientations of the patch antenna were taken.

7.4.2 Results

Despite the testing conditions not being ideal, we can see some interesting results in the following graphs.

In Figure 23 the measurements of S_{21} for different orientations of the antenna are presented, in the desired frequency range. The plotted lines were smoothed using moving average.

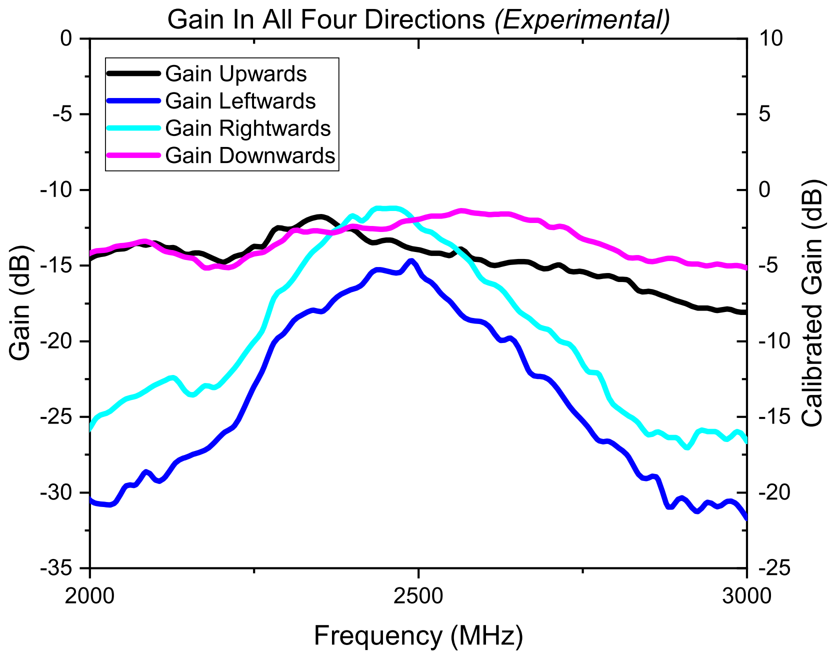

***Figure 23**: S_{21} Graph in different polarization angles*

Using the data from Figure 23, we can derive the experimental gain by averaging the measurements from the two parallel planes *(Left with Right and Up with Down)* and then calculate the following:

$$20 * \log_{10}\left(\sqrt{G_{LR} + G_{UD}}\right) \tag{1}$$

where G_{LR} is the average gain from the right and left directions and G_{UD} is the gain from the up and down directions. All gain used in the equation above are expressed in pure number and not in dB. If we calculate the expression above for each data point then we end up with the following Figure 24, showing the calculated gain along with the theoretical acquired from the simulations.

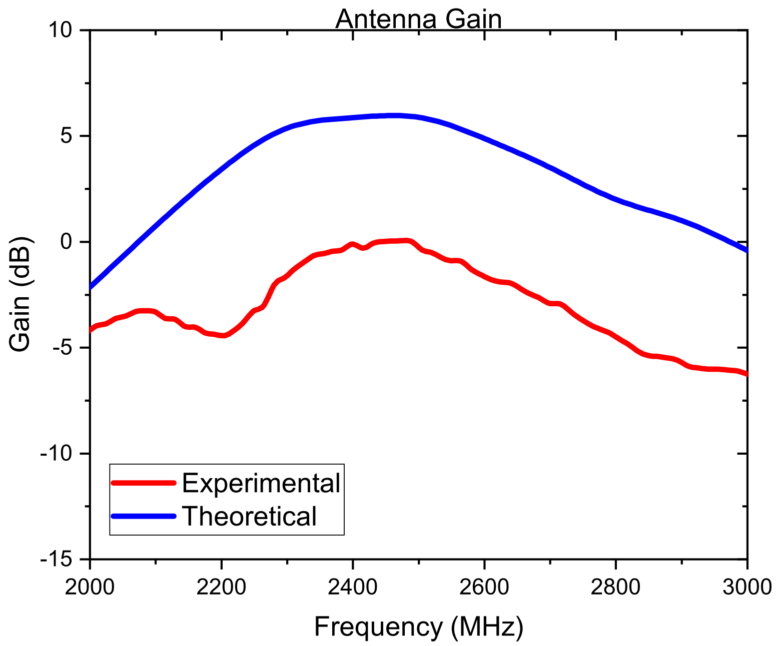

Figure 24: *Theoretical vs. Calculated antenna gain*

For comparison purposes, the gain of a dipole was measured and is shown in Figure 25.

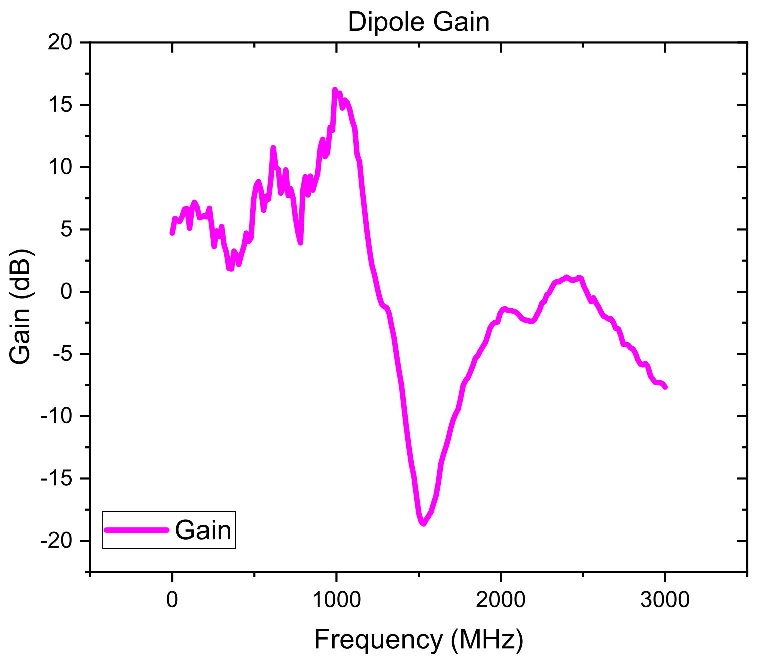

Figure 25: *Reference Dipole gain*

Having calculated the gain before as G_{LR} and G_{UD}, not in dB, we can calculate the ratio as:

$$20 * \log_{10}\left(\frac{G_{UD}}{G_{LR}}\right) \tag{2}$$

giving us the axial ratio of the antenna. The result of this calculation for each data point is illustrated in Figure 26. A horizontal line is also visible, indicating the 3 dB margin where the polarization is considered circular.

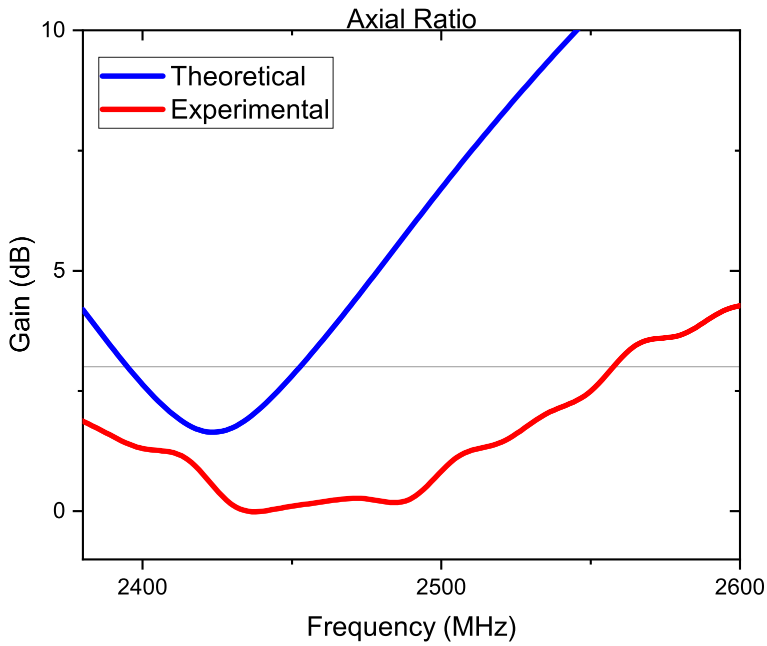

***Figure 26**: Patch axial ratio experimental vs. theoretical*

7.5 Reflection coefficient (S_{11}) measurement

The antenna was connected to one of the ports of the network analyzer. The data points of the S_{11} measurement are illustrated in Figure 27.

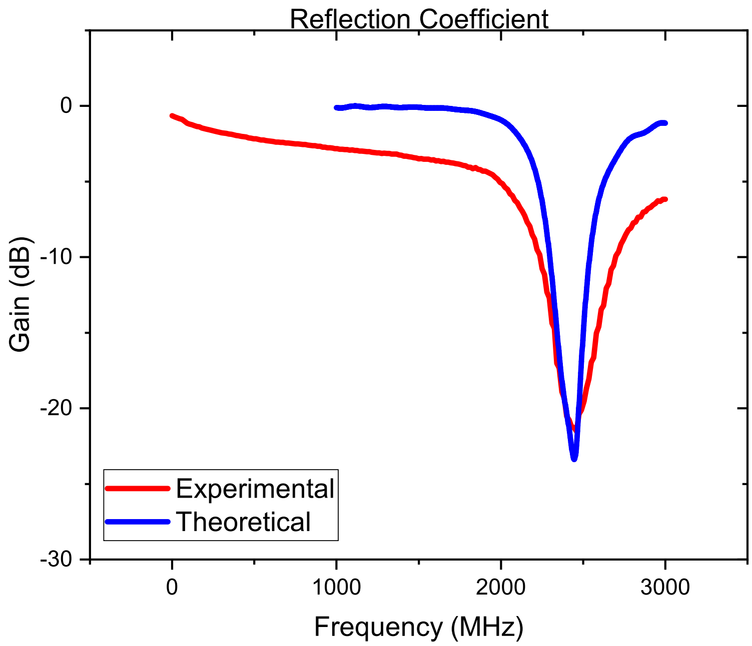

***Figure 27**: S_{11} Reflection coefficient*

7.6 Conclusions

- The axial ratio of the antenna appears improved in comparison to the theoretical value, as it bellow the 3 dB margin for a larger bandwidth and approximates 0 dB in some cases (Figure 26).
- The reflection coefficient result indicates that, when considering a -10 dB limit, the antenna is operational at a larger bandwidth than expected (*~800 MHz experimental vs ~200 MHz theoretical*) (Figure 27).
- The gain measurement is almost 5 dB lower than the simulated value (Figure 24). Given that the reference dipole gain approximates its expected value in the frequency range of interest, the experimental results are deemed to be reliable, even though being preliminary. The broader operational bandwidth (Figure 27) translates to reduction of the antenna's quality factor Q and consequently in degradation of the gain, since a lower Q indicates greater power losses in the antenna.The Q factor is dependant on the antenna's substrate thickness and for that reason the multilayer substrate may be responsible for the aforementioned remarks. Further optimization of the design is deemed necessary and testing in an electromagnetically isolated environment (e.g. anechoic chamber) will aid in that direction.

8 Anechoic chamber testing

8.1 Measurement conditions

The measurements were carried out in the anechoic chamber of the Radar and Microwaves Unit of the Electrical and Computer Engineering School, in Aristotle University of Thessaloniki, with the aid of the personnel of the unit.

Due to the absorbing material in the chamber as well as the available equipment in the lab, frequencies starting from approximately 800 MHz and above can be measured.

The main limitation we had during the testing was that it was the first time that a circular polarization antenna was to be measured in the anechoic chamber, and no circular polarization antenna for the receiving end was available. Nevertheless, we found alternative ways to extract the desired characteristics, which are presented in detail in the following sections.

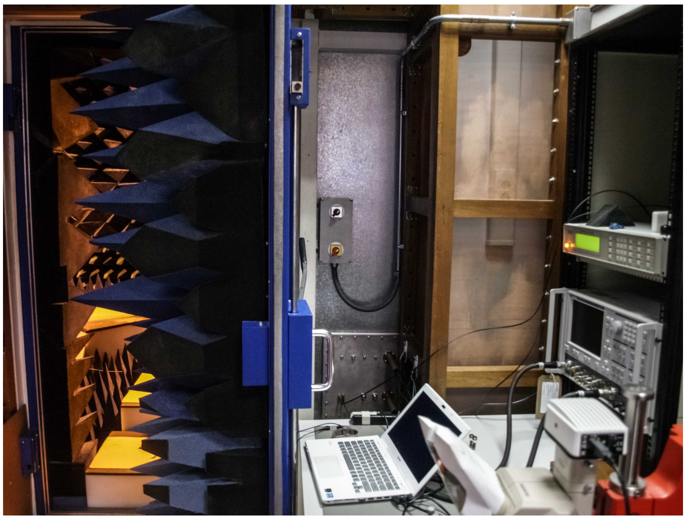

Figure 28: *The entrance to the chamber and the supporting equipment for conducting measurements*

8.2 Measurement equipment

The equipment used for the measurements was the following:

- *Anritsu 37397D* Vector Network Analyzer (Figure 29)

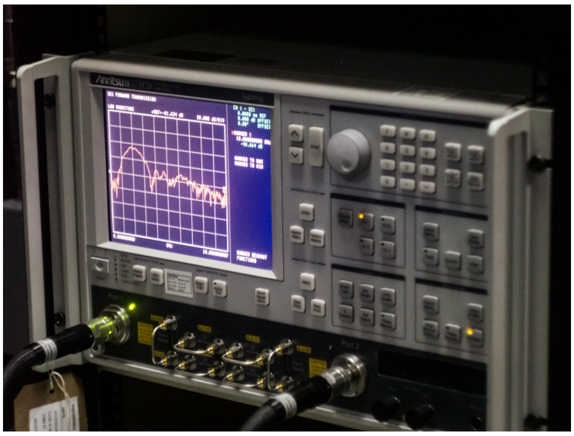

Figure 29: *The Anritsu 37397D VNA that was used for the measurements*

- Two *L3HARRIS* standard gain horn antennas (the gain curve can be found here)

Figure 30: *L3HARRIS standard gain horn antennas*

- DE3600 turning device (Figure 31)

8.3 Directivity measurement

8.3.1 Procedure

The AUT was mounted on a rotating base which could be turned from -90 to 90 degrees, as seen in Figure 31. Two sweeps while **measuring** S_{21} were performed:

- A sweep with the slot of the AUT facing up
- A sweep with the slot of the AUT facing right, 90° with respect to the first measurement (Figure 33)

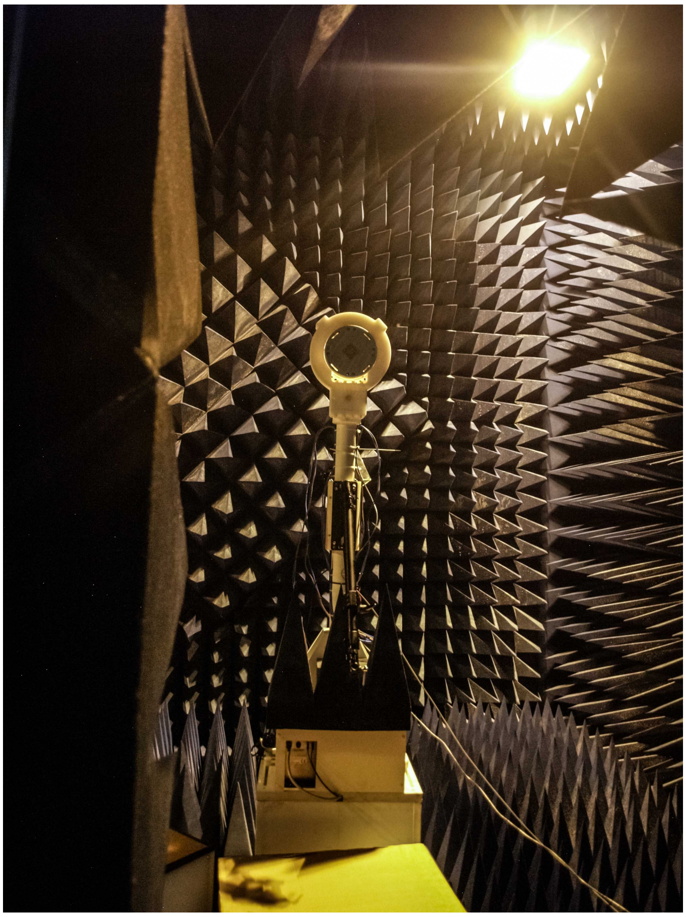

***Figure 31**: Rotating base of the anechoic chamber*

On the receiving end, the standard gain horn antenna was used, mounted on a fixed tripod (Figure 32).

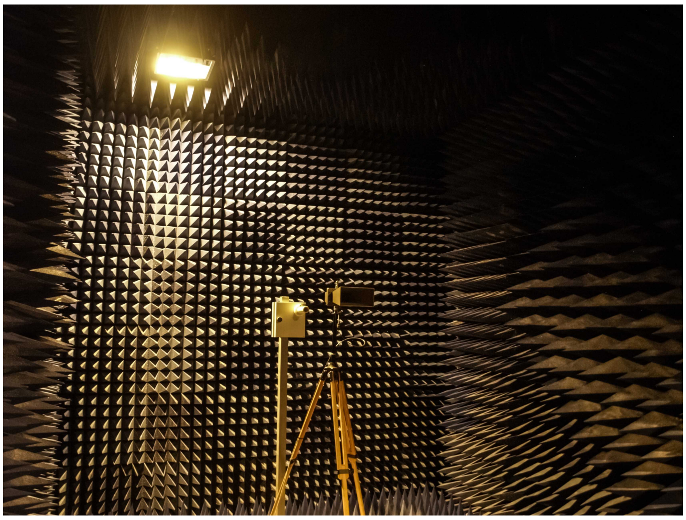

***Figure 32**: Horn antenna base at the other end of the chamber*

Both measurements had an averaging of **1 second** and an angular step of **1°**. The

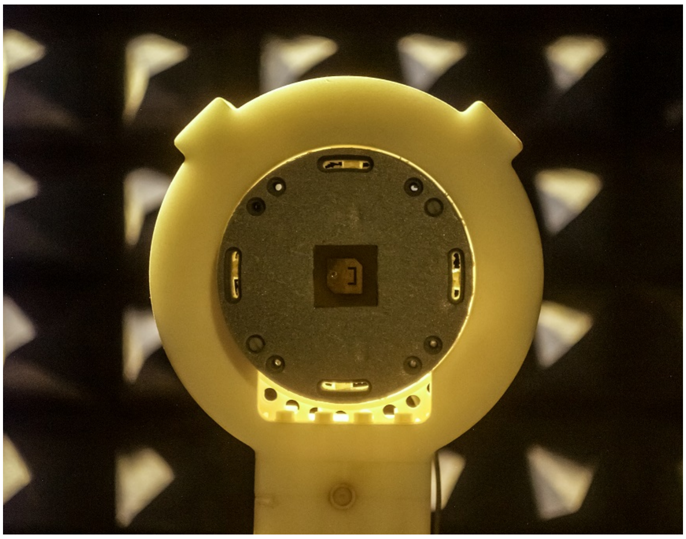

***Figure 33**: Close-up of the holding base*

reason we repeated the measurement for two different orientations of the AUT was due to the horn antenna being linearly polarized. Since the polarization of the AUT is supposedly circular, the total electric field vector consists of two perpendicular, linearly polarized components with a 90° phase difference between them. These two "slices" were used to calculate the antenna pattern in 2D and 3D space.

8.3.2 Data analysis

The 3D pattern reconstruction was done using the data from the two slices, by the cross-weighted method. Each point of the the slices was multiplied by the complement value, in linear space, of the other slice at the same angle. This way a weight matrix was formed and then the points were added together. A better visualization of the process can be seen in the code of this notebook.

8.3.3 Results

The final results are almost 100% compliant with the simulation, providing **104 degrees** of HPBW and a directivity of **5.95 dB**. In Figure 34 the reconstructed 3D antenna pattern can be found, highlighting the directivity of the antenna in 3D space.

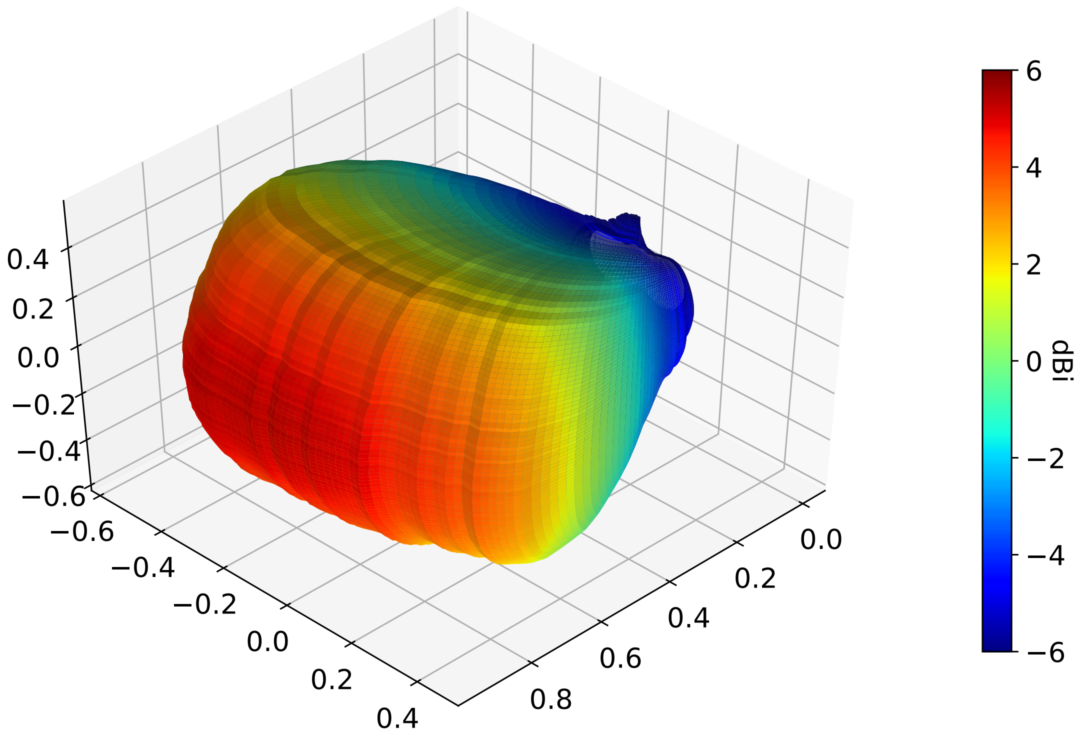

***Figure 34**: Measured 3D directivity of the patch antenna*

A better overview of the actual pattern is provided by the slices in Figure 35 and Figure 36.

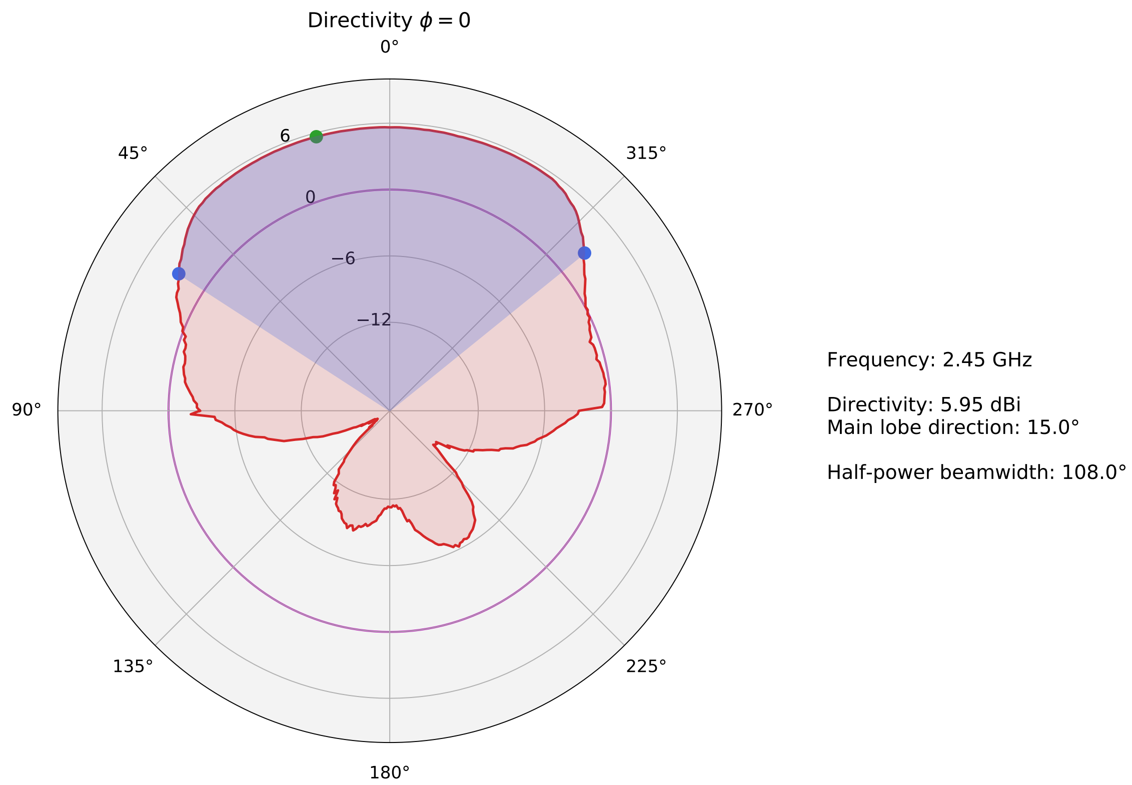

***Figure 35**: Measured 2D radiation pattern of the patch antenna ($\phi = 0$)*

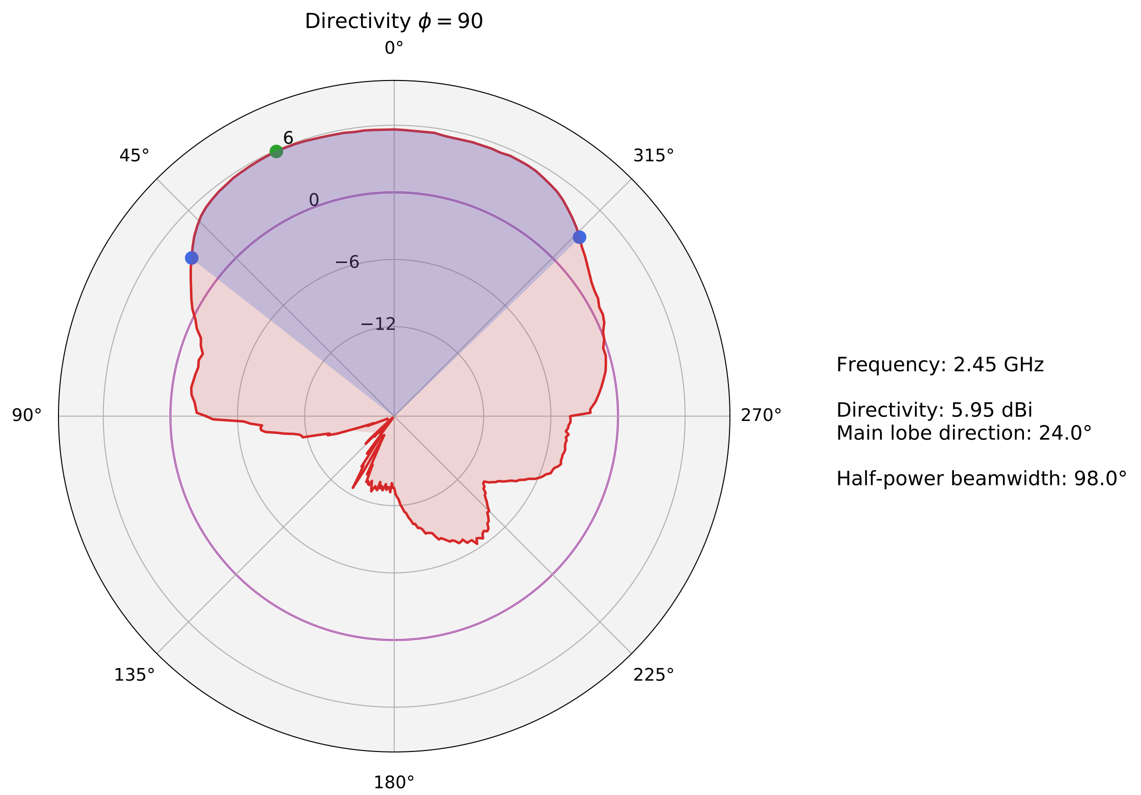

***Figure 36**: Measured 2D radiation pattern of the patch antenna ($\phi = 90$)*

8.4 Gain measurement

8.4.1 Procedure

In order to measure the gain of the antenna, we followed a procedure of reference calibration, similar to the one described in subsubsection 7.4.1. Namely, we used two standard gain horn antennas on fixed tripods, facing one another (as portrayed in Figure 37), each one connected to a port in the VNA. We measured the S_{21} in the range **2-3 GHz** to be used as calibration and afterwards proceeded on replacing one of the horns with the AUT, as illustrated in Figure 38. We then repeated the S_{21} measurement with the latter configuration for 4 directions of the AUT (slot facing up, down, left and right).

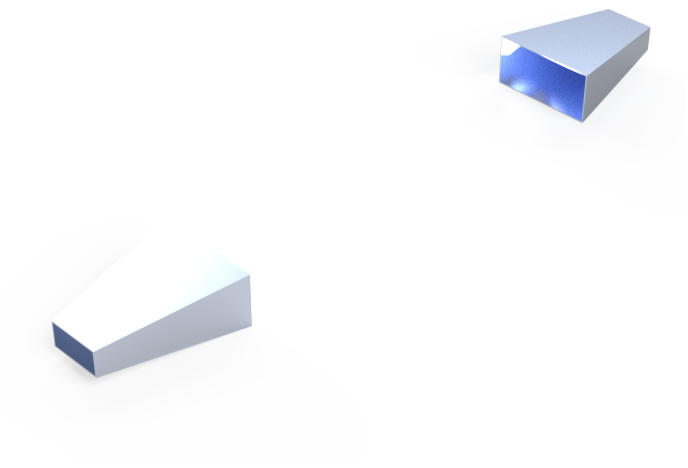

***Figure 37**: Reference calibration layout*

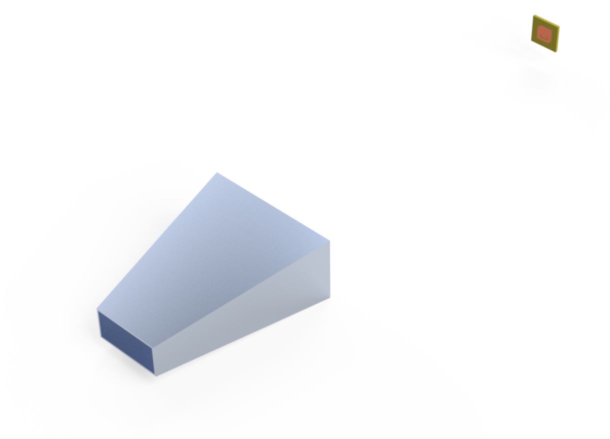

***Figure 38**: Actual antenna measurement*

8.4.2 Data analysis

Due to the larger dimensions of the horn antenna, there was a displacement of its face by **r=29cm** with respect to the AUT, thus giving slightly higher readings. We compensated for that by calculating the value that we need to deduct from the measurement using the Friis law as follows:

$$S_{21}^{patch} = G_{patch} + G_{horn} + 20\log\left(\frac{\lambda}{4\pi(D+r)}\right), \tag{3}$$

$$S_{21}^{horn} = 2G_{horn} + 20\log\left(\frac{\lambda}{4\pi D}\right), \tag{4}$$

and the gain of the AUT was calculated as

$$S_{21}^{patch} - S_{21}^{horn} = G_{patch} - G_{horn} + 20\log\left(\frac{\lambda}{4\pi(D+r)}\right) - 20\log\left(\frac{\lambda}{4\pi D}\right) \Rightarrow$$
$$\Rightarrow \boxed{G_{patch} = S_{21}^{patch} - S_{21}^{horn} + G_{horn} + 20(\log(D+r) - \log D)},$$

where **D=1.4m** is the total distance of the reference horn from the measurement horn.

Since we had 4 different S_{21} measurements (one for each direction of the AUT), we extracted the mean value in the vertical and horizontal dimensions as

$$S_{21_{VER}}^{patch} = \frac{S_{21_{DOWN}}^{patch} + S_{21_{UP}}^{patch}}{2} \tag{5}$$

and similarly

$$S_{21_{HOR}}^{patch} = \frac{S_{21_{LEFT}}^{patch} + S_{21_{RIGHT}}^{patch}}{2}. \tag{6}$$

Now, assuming perfect circular polarization, we calculated S_{21}^{patch} as:

$$S_{21}^{patch} = \sqrt{\left(S_{21_{VER}}^{patch}\right)^2 + \left(S_{21_{HOR}}^{patch}\right)^2}. \tag{7}$$

Finally, to compensate for the imperfect circular polarization, the phase measurements were used to calculate the polarization loss (Figure 45), as explained in subsection 8.5. The end result yields:

$$S_{21}^{patch-comp} = S_{21}^{patch} + Polarization\ Loss \tag{8}$$

8.4.3 Results

The graph shown in Figure 39, clearly indicates the gain at different values of the frequency. Within the desired frequency range, **2.4 - 2.45 GHz**, the gain fluctuates from **4 - 4.15 dB**, which is more than acceptable for the mission.

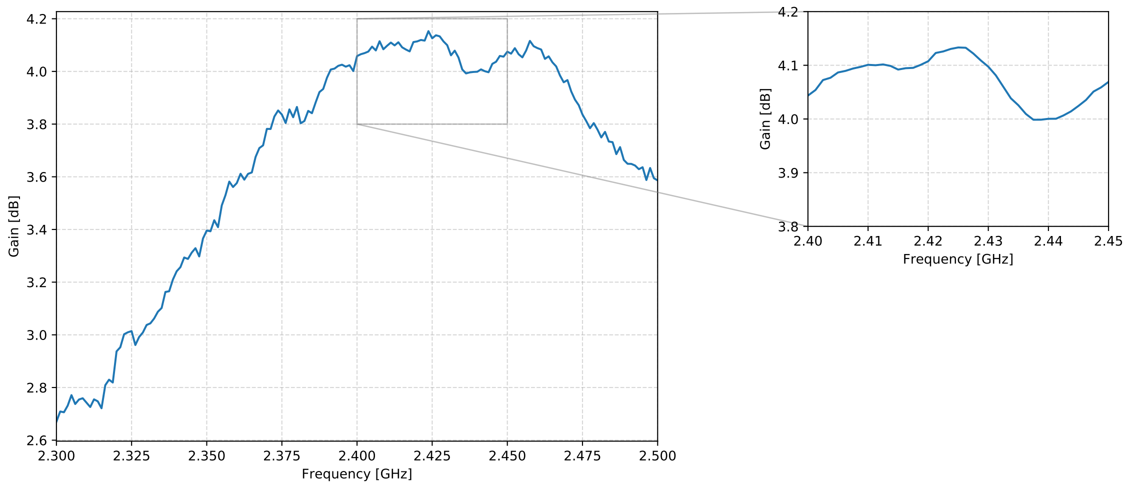

***Figure 39**: Patch antenna gain vs frequency*

The analysis notebook can always be found on GitLab.

Also for better visualization of the gain on antenna pattern, the following Figure 40 and Figure 41 can be used. To get this diagram, the normalized version of the Figure 36 and Figure 35 respectively was used and then multiplied by the value extracted from Figure 8 for **2.425 GHz**.

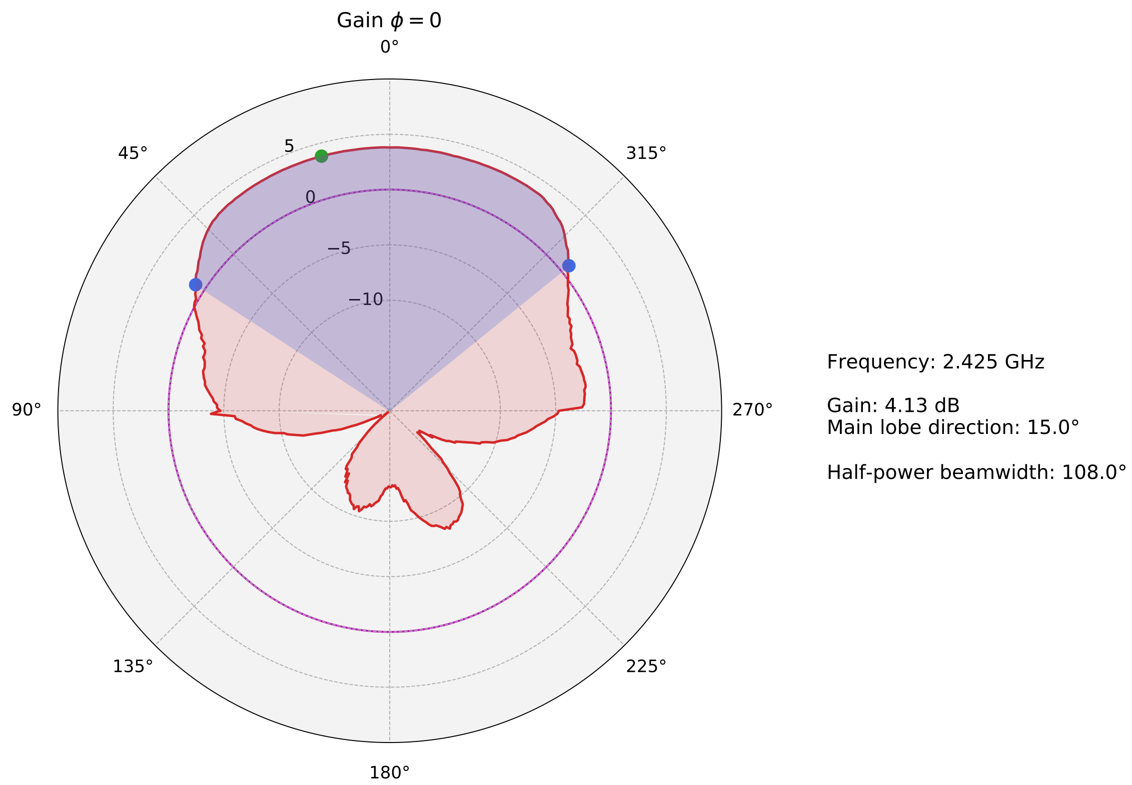

***Figure 40**: Patch antenna gain pattern ($\phi = 0$)*

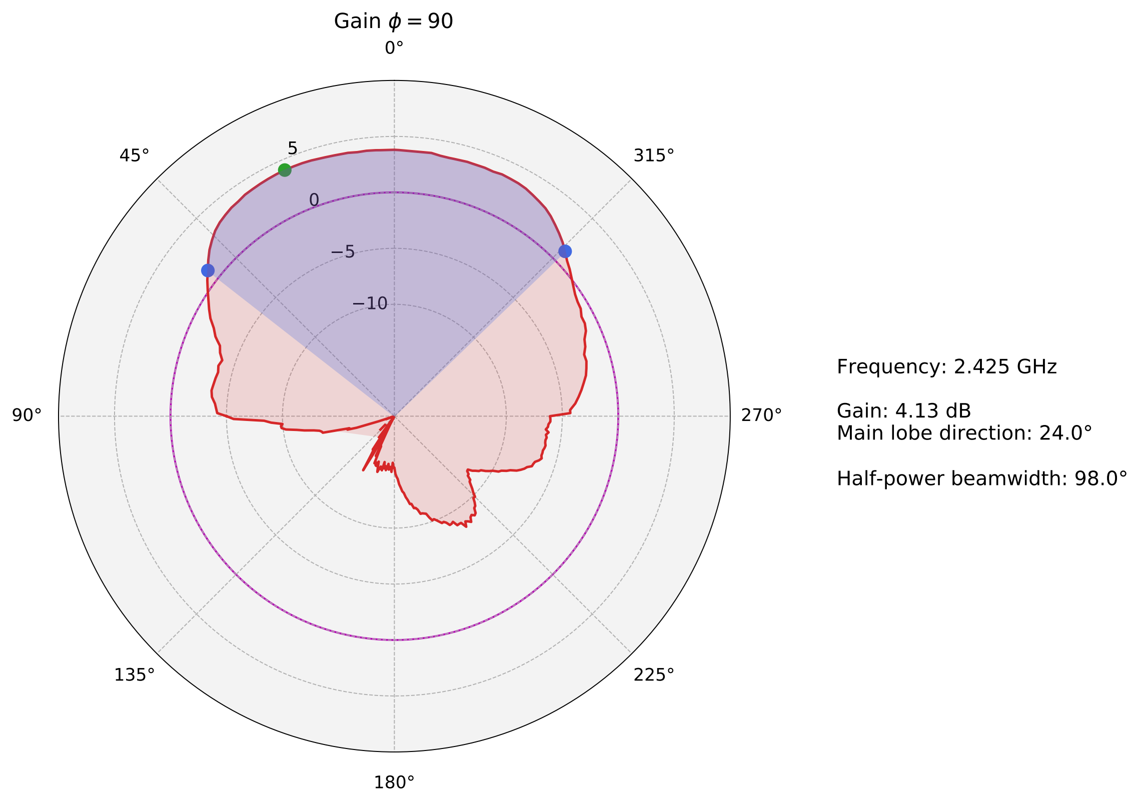

***Figure 41**: Patch antenna gain pattern ($\phi = 90$)*

8.5 Phase measurement

To conclude the testing, we had to also take phase into account. In reality, no antenna is perfectly circularly polarized but rather elliptically polarized, either due to the magnitude of the two linear electric field components not being equal (as was the case with our measurements in the previous sections), or due to the phase difference not being exactly 90°.

8.5.1 Procedure

The setup and procedure of the phase measurement was almost identical to the ones described in subsubsection 8.3.1, with the differences being that:

- instead of S_{21}, the VNA was set to measure the phase component of the singal
- the measurements were extracted for 4 different orientations of the AUT, same as in subsubsection 8.4.1

8.5.2 Data analysis

The first and simplest analysis to be conducted is to calculate the phase difference between the horizontal and the vertical component of the phase. This will indicate the polarization direction, either left *(+)* or right *(-)*, by the sign of the difference.

Phase measurements can provide an insight for the axial ratio and the polarization mismatch loss between the receiving and the transmitting antenna. To calculate the axial ratio, we need to convert the measured orthogonal components to the actual frame of an ellipse.

The analysis was based on [3] and the calculation of the respective angles can be found on GitLab in the notebook named `Patch_Antenna_Phase.ipynb`. In Figure 42 the polarization ellipse is shown, with all the required angles and notations used in the analysis. Using angle χ, the ratio of the ellipse semi-axis was calculated and by using both χ and ψ angles the points on the Poincare sphere were determined.

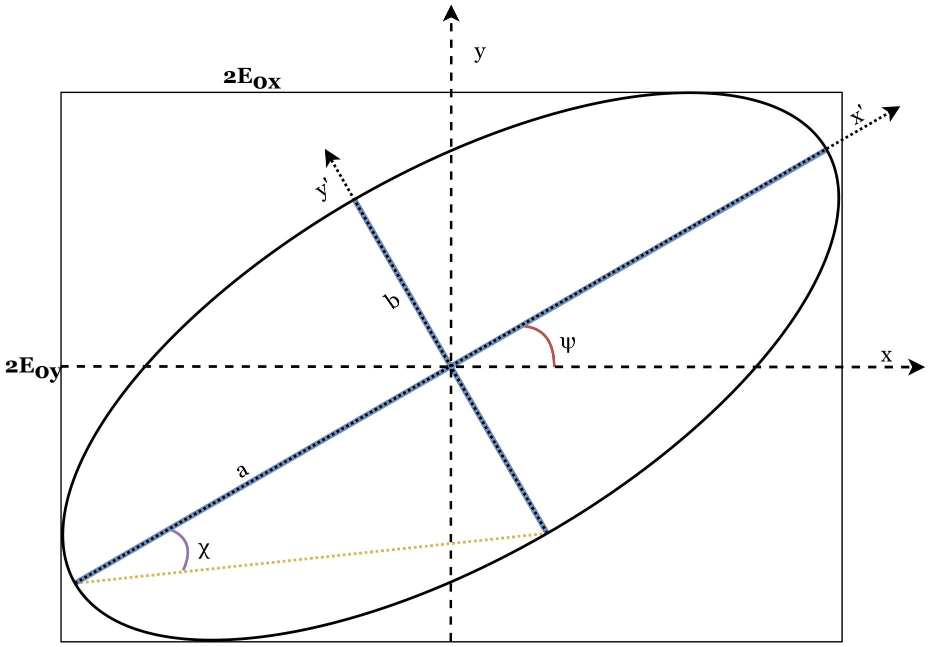

***Figure 42**: Polarization ellipse*

For better visualization of some graphs, the polarization ellipse based analysis can be found in [6], where the angle notation changes. Both [3] and [6] were used to better understand the theory behind the Poincare sphere and the polarization ellipse.

8.5.3 Results

As it can be seen in Figure 43 the phase difference decreases, but it is positive indicating a left hand polarized antenna. As mentioned earlier, in order to understand the antenna behavior in terms of the polarization at different angles and at different frequencies, we need to dig deeper than just taking the phase difference. Such results can be seen in Figure 44 and Figure 45, where the axial ratio of the antenna and the polarization loss *(considering a left hand circularly polarized antenna)* can be seen respectively.

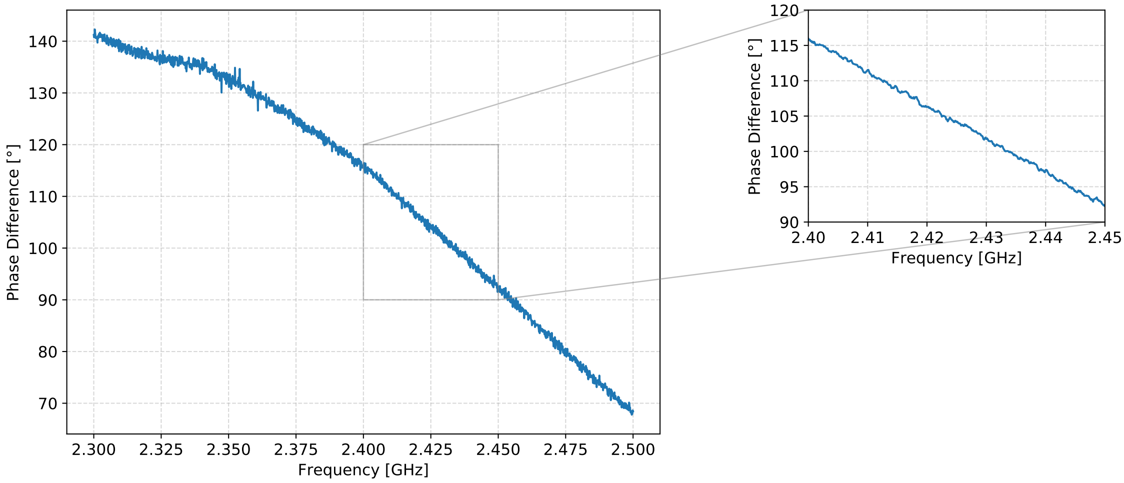

Figure 43: *Phase difference in different frequencies*

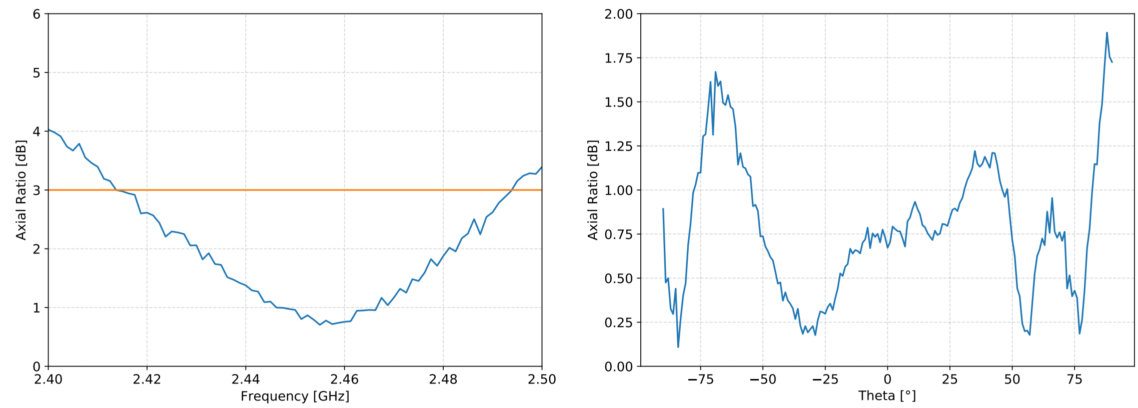

Figure 44: *Axial ratio of the antenna. The angle diagram is @ 2.45 GHz*

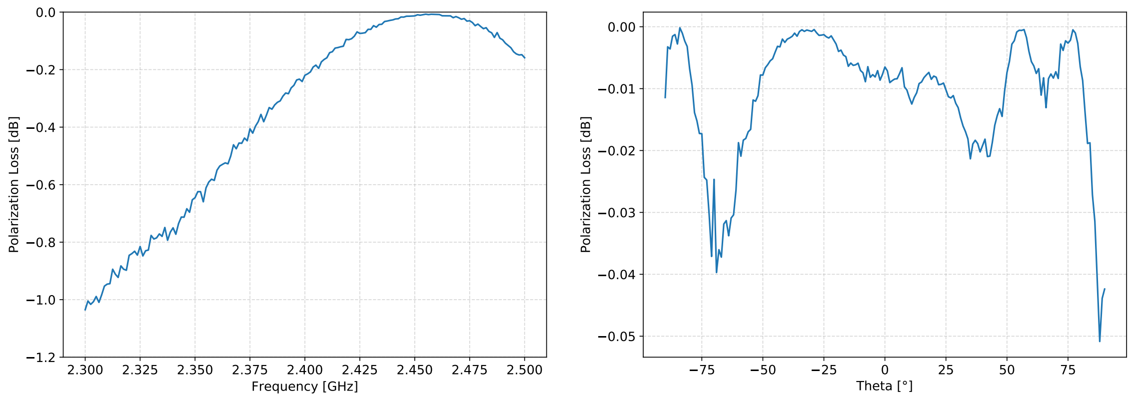

Figure 45: *Polarization mismatch loss considering left hand circularly polarized receiving antenna. The angle diagram is @ 2.45 GHz*

8.6 Reflection coefficient measurement

The AUT was connected to one port of the VNA. The result is presented in Figure 46.

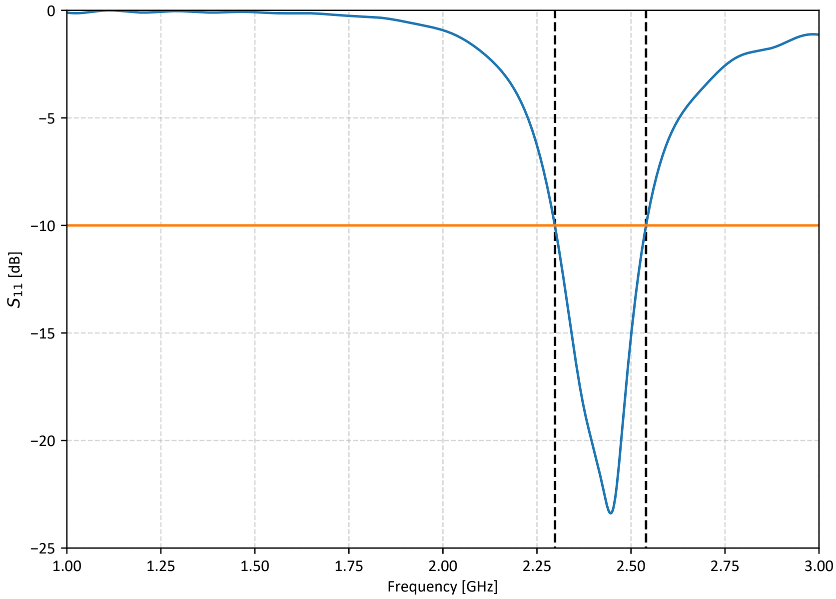

***Figure 46**: Measured reflection coeffient*

8.7 Conclusions

It is prevalent from this report that the process from design to actual construction is a tricky one, with many pitfalls along the way. The main conclusions we drawn after the tests conducted in the anechoic chamber were:

- In the frequeny range of interest (2.4-2.45 GHz), the effect of the surrounding environment on the transmission coefficient measurements is considerably impactful (as can be deducted by the difference with the results of the preliminary testing). This fact is probably caused by the widespread usage of the aforementioned frequencies for S band ISM applications (e.g. Wi-Fi).
- The reflection coefficient measurement is almost independent of the measurement circumstances
- The antenna is slightly less directional with respect to the simulations (boader HPBW, smaller maximum gain)

9 Open issues

There are some open issues that need to be addressed in the future:

- Test the actual model, with the screws attached and the antenna on the frame (Figure 47) in the anechoic chamber, to check if there is any noticeable difference. It is worth mentioning though that the simulation have shown no significant difference with the antenna places on the frame with four screws in the corners.

***Figure 47**: Frame render with patch antenna*

- Measure the phase with respect to angle for the 2.4 GHz frequency as well
- Add simulations of the patch antenna mounted on the frame in the report

A Mechanical drawings

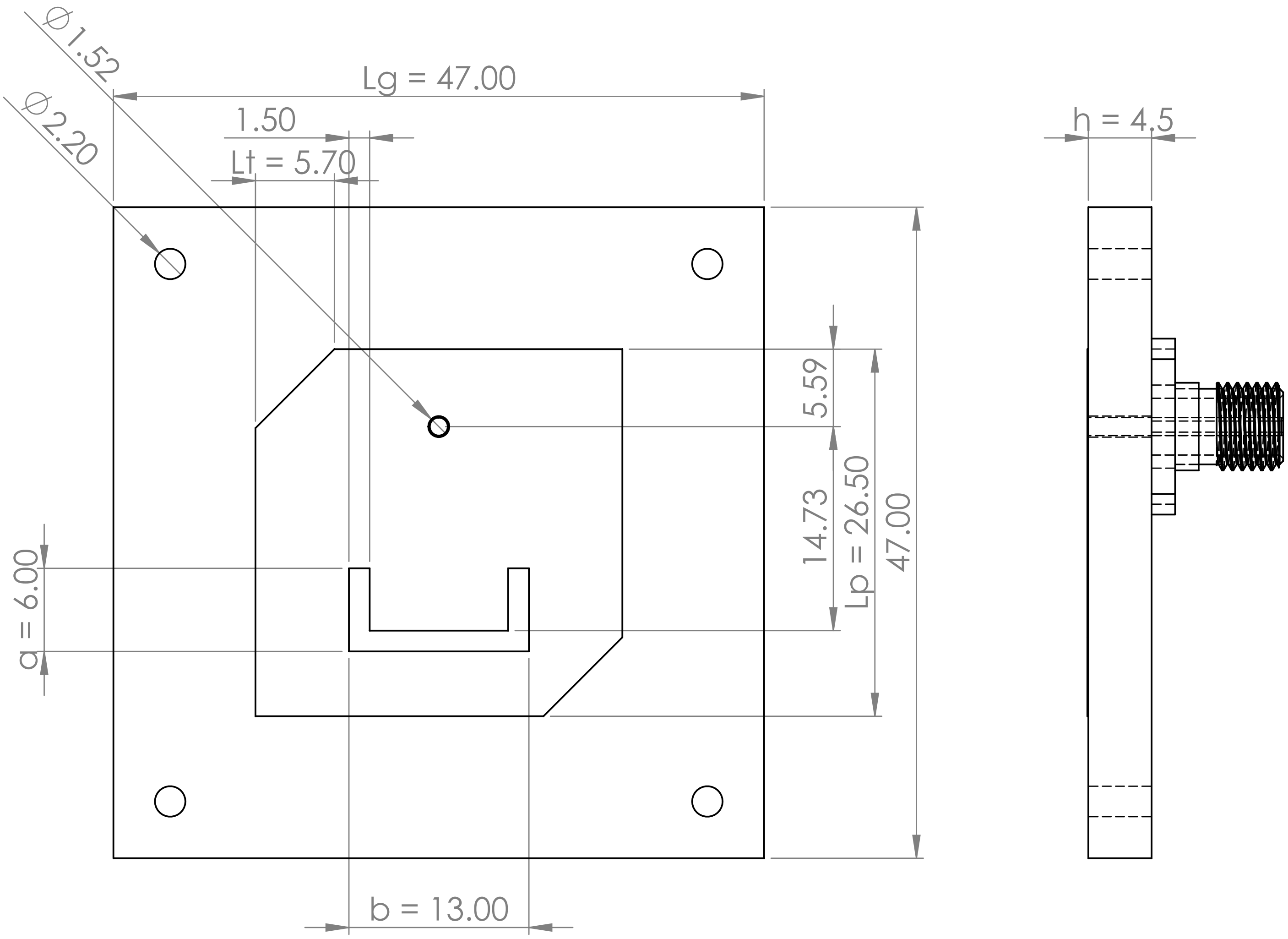

***Figure 48**: 2.4GHz Patch Antenna Mechanical Drawings. All dimensions displayed are in mm.*

B Document-ID reference

AcubeSAT - COM - G - 011 2

Version number

Document number

Category:
- E: Experimentation & Development
- B: Research & Technical Background
- M: Meeting Outcomes
- T: Technical Specification
- G: Technical Guides & Handbooks
- O: Generic & Operational

Subsystem:
- GEN: General
- ADC: Attitude Determination & Control
- COM: Communications
- EPS: Electrical Power
- OBC: On-board Data Handling
- OPS: Spacecraft Operations
- SCI: Science Unit
- STR: Structural
- SYE: Systems Engineering
- THE: Thermal
- TRA: Trajectory
- COL: Collaboration
- PRG: Programmatic

For more information, see https://helit.org/mm/docList/public/categories